INTERNATIONAL JOURNAL FOR NUMERICAL METHODS IN FLUIDS
Int. J. Numer. Meth. Fluids 2007; **54**:1055–1074
Published online 21 December 2006 in Wiley InterScience (www.interscience.wiley.com). DOI: 10.1002/fld.1414

An implicit two-dimensional non-hydrostatic model for free-surface flows

Afshin Ahmadi*,†,‡, Peyman Badiei§ and Masoud M. Namin§

Faculty of Civil Engineering, School of Engineering, University of Tehran, P.O. Box 11365-4563, Tehran, Iran

SUMMARY

An implicit finite volume model in sigma coordinate system is developed to simulate two-dimensional (2D) vertical free surface flows, deploying a non-hydrostatic pressure distribution. The algorithm is based on a projection method which solves the complete 2D Navier–Stokes equations in two steps. First the pressure term in the momentum equations is excluded and the resultant advection–diffusion equations are solved. In the second step the continuity and the momentum equation with only the pressure terms are solved to give a block tri-diagonal system of equation with pressure as the unknown. This system can be solved by a direct matrix solver without iteration. A new implicit treatment of non-hydrostatic pressure, similar to the lower layers is applied to the top layer which makes the model free of any hydrostatic pressure assumption all through the water column. This treatment enables the model to evaluate both free surface elevation and wave celerity more accurately. A series of numerical tests including free-surface flows with significant vertical accelerations and nonlinear behaviour in shoaling zone are performed. Comparison between numerical results, analytical solutions and experimental data demonstrates a satisfactory performance.

Received 30 May 2006; Revised 17 October 2006; Accepted 24 October 2006

KEY WORDS: projection method; implicit finite volume method; non-hydrostatic pressure; free-surface flow; sigma coordinate; top layer treatment

1. INTRODUCTION

Numerical simulation of free-surface flows based on incompressible Navier–Stokes equations (NSE) is extensively applied in river, estuarine and coastal studies. With the rapid increase in

*Correspondence to: Afshin Ahmadi, Faculty of Civil Engineering, School of Engineering, University of Tehran, P.O. Box 11365-4563, Tehran, Iran.
†E-mail: afahmadi@ut.ac.ir
‡PhD candidate.
§Assistant Professor.

Contract/grant sponsor: Water Resources Management Co.; contract/grant number: RIV1-83084
Contract/grant sponsor: Faculty of Civil Engineering, School of Engineering, University of Tehran

computer power in recent years, three-dimensional (3D) models are extensively developed and applied for such problems. One of the main difficulties of such models is the proper handling of free surface moving boundary, especially for the cases such as short period waves. The moving free surface forms the upper boundary of the computational domain; however, its position also constitutes a part of the solution yet to be defined. In many 3D free-surface models, it is assumed that the vertical acceleration is small so that the idea of hydrostatic pressure can be applied. However, this statement is only applicable for simulating flows where the horizontal scale of motion is much larger than its vertical scale. For cases such as short period waves, rapidly changing bed topographies, and stratification due to strong density gradients, the hydrostatic pressure distribution is no longer valid and employing a dynamic pressure distribution, based on the complete form of NSE, is indispensable.

In recent years, the development of non-hydrostatic models has been the topic of many research activities. Chorin [1] developed an explicit projection method that obtains the projected intermediate velocities after solving advection and diffusion terms explicitly at each time step, and then corrects the projected velocities by solving the pressure Poisson equation (PPE). Although the projection method may cause splitting errors in some applications [2], it has the advantage of using different schemes for different stages. Mahadevan *et al*. [3] proposed a non-hydrostatic ocean model using a semi-implicit control volume method. Stansby and Zhou [4] developed a two-dimensional (2D) vertical flow model for simulating the non-hydrostatic problem, using a semi-implicit time stepping method. Casulli [5] planned a semi-implicit, fractional step technique which obtained the non-hydrostatic pressure in two steps. Other recent developments in the non-hydrostatic models can be found in Li and Fleming [6], Lin and Li [7], Kocyigit *et al*. [8] and Chen [9]. Recently a fully non-hydrostatic implicit algorithm based on finite difference scheme was suggested by Namin *et al*. [10, 11] and Yuan and Wu [12, 13]. The algorithm solves the NSE and the free-surface boundary condition simultaneously and forms a block tri-diagonal system with the unknown horizontal velocity. Consequently a direct matrix solver can be applied without any iteration.

Many non-hydrostatic models [3, 6, 10, 11, 14] use hydrostatic pressure assumption at the top layer. In these models, a large number of vertical layers are necessary to simulate non-hydrostatic free-surface flows [15] and in particular wave propagation. Some models proposed a correction to the hydrostatic relation at the top layer [5, 9, 16]. The non-hydrostatic pressure at top-layer has not been correctly applied in models based on PPE or projection method. Yuan and Wu [12, 13] planned an integral technique to remove the top-layer hydrostatic assumption under a staggered grid framework. In their model, the vertical momentum equation is integrated from the centre of the top layer to the moving free surface. The top-layer pressure is expressed as a function of the free-surface elevation (hydrostatic pressure component) and the vertical acceleration (non-hydrostatic pressure component). Their results demonstrate that by applying non-hydrostatic pressure distribution to the top layer, phase errors are noticeably reduced in the simulation of dispersive waves.

Since in two-dimensional (2DV) and 3D non-hydrostatic problems, the size of the resulting system of equations is large, the simulation time becomes a restricting criterion. In some models, iterative algorithms are deployed to solve the matrix system which is time consuming [5–7, 15]. More recently for 2DV implicit algorithms Namin *et al*. [10, 11] proposed a method that yields a block tri-diagonal system of equation which can be solved without any iteration and save the computational cost.

In this paper, a finite volume model for solving the 2D free-surface flow in the vertical plane is presented. Unlike the finite difference models developed by Namin *et al*. [10] and Yuan and Wu [12] in which the equations are solved simultaneously in one stage, the algorithm of current

DOI: 10.1002/fld

work is based on projection method which solves the complete 2D Navier–Stokes equations in two steps. First the pressure term in the momentum equations is excluded and the resultant advection–diffusion equations are solved. In the second step the continuity and the momentum equation with only the pressure term are solved to give a block tri-diagonal system of equation with pressure as the unknown. This system of equations can be solved by a direct matrix solver without iteration. Since the main bulk of the CPU time is spent for second step, deploying time splitting method and excluding nonlinear terms in this step reduces the size of matrix system noticeably and decreases the execution time as compared to Namin *et al.* [10] and Yuan and Wu [12] models. Furthermore, one is free to use different numerical schemes for each stage. With this algorithm, the kinematic free-surface boundary condition is solved simultaneously with the momentum and continuity equations in second step, so that the water elevation can be obtained along with the velocity and pressure fields as a part of the solution. The sigma coordinate grid system has been chosen as the computational mesh, which enables the model to simulate free-surface flows over irregular geometries. The model is capable of simulating free-surface flows without using hydrostatic pressure assumption at the centre of free-surface layer. A non-hydrostatic pressure approximation for free-surface cells is derived, which calculates pressure gradient and vertical accelerations by implementing free surface dynamic and kinematic boundary conditions. This method which is different from that of Yuan and Wu [12] enables the model to simulate both free surface elevation and wave celerity more accurately.

Section 2 presents the governing equations together with boundary conditions. The numerical method is explained in Section 3. In Section 4, the model is validated by four tests, including a linear progressive short wave, solitary wave propagation over constant and variable water depths and nonlinear progressive short waves. Numerical results are compared with analytical solutions or experimental data to show the validity and accuracy of the model.

2. MATHEMATICAL FORMULATION

The governing equations used to describe the 2D vertical, incompressible flows are continuity and momentum equations. Figure 1 shows the physical domain bounded by the moving free surface, $z = \xi(x, t)$, and the bottom, $z = -h(x, t)$. The conservative form of the equations is expressed as

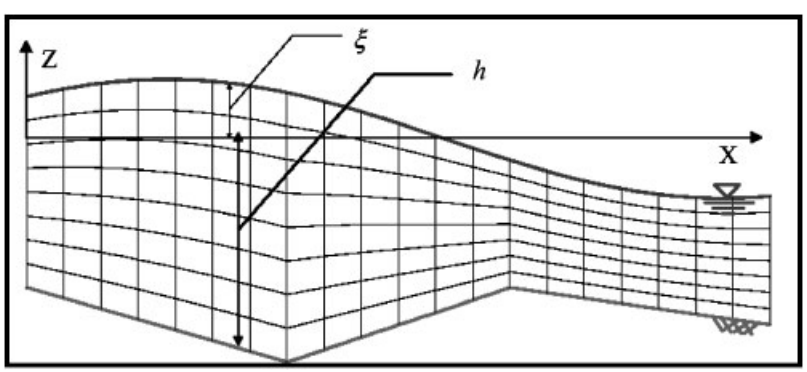

Figure 1. Sigma coordinate system with uniform grid size over depth deployed for 2DV calculations.

DOI: 10.1002/fld

follows:

$$\frac{\partial u}{\partial x}+\frac{\partial w}{\partial z}=0 \tag{1}$$

$$\frac{\partial u}{\partial t}+\frac{\partial u^2}{\partial x}+\frac{\partial uw}{\partial z}+\frac{1}{\rho}\frac{\partial P}{\partial x}=\frac{\partial}{\partial x}\left(v_t\frac{\partial u}{\partial x}\right)+\frac{\partial}{\partial z}\left(v_t\frac{\partial u}{\partial z}\right) \tag{2}$$

$$\frac{\partial w}{\partial t}+\frac{\partial uw}{\partial x}+\frac{\partial w^2}{\partial z}+\frac{1}{\rho}\frac{\partial P}{\partial z}=\frac{\partial}{\partial x}\left(v_t\frac{\partial w}{\partial x}\right)+\frac{\partial}{\partial z}\left(v_t\frac{\partial w}{\partial z}\right)-g \tag{3}$$

where t is time; x, z are coordinates in horizontal and vertical directions, respectively; u, w are components of velocity in the x and z directions, respectively; P is pressure; ρ is the density of water; g is the gravitational acceleration; and v_t is the eddy viscosity coefficient.

The pressure has been divided here into two parts namely, the 'hydrostatic pressure' and 'excess pressure' (ρP^*) as

$$P=-\rho gz+\rho P^* \tag{4}$$

Substituting Equations (4) in Equations (2) and (3), the 2DV momentum equations can be written in the form

$$\frac{\partial u}{\partial t}+\frac{\partial u^2}{\partial x}+\frac{\partial uw}{\partial z}+\frac{\partial P^*}{\partial x}=\frac{\partial}{\partial x}\left(v_t\frac{\partial u}{\partial x}\right)+\frac{\partial}{\partial z}\left(v_t\frac{\partial u}{\partial z}\right) \tag{5}$$

$$\frac{\partial w}{\partial t}+\frac{\partial uw}{\partial x}+\frac{\partial w^2}{\partial z}+\frac{\partial P^*}{\partial z}=\frac{\partial}{\partial x}\left(v_t\frac{\partial w}{\partial x}\right)+\frac{\partial}{\partial z}\left(v_t\frac{\partial w}{\partial z}\right) \tag{6}$$

Since the bottom surface may not be regular, the kinematic boundary condition at the impermeable bottom is

$$u\frac{\partial h}{\partial x}+w=0 \tag{7}$$

Similarly, the kinematic boundary condition at the moving free surface is

$$\frac{\partial \xi}{\partial t}+u\frac{\partial \xi}{\partial x}=w \tag{8}$$

where ξ is the surface elevation. Integrating the continuity equation (1) over the water depth and applying the Leibniz's rule with the kinematic boundary conditions (7) and (8) gives the free-surface equation

$$\frac{\partial \xi}{\partial t}+\frac{\partial}{\partial x}\int_{-h}^{\xi}u\,\mathrm{d}z=0 \tag{9}$$

2.1. Boundary conditions

At impermeable bottom and wall boundaries zero normal velocity is applied. For viscous flows no-slip boundary condition is considered. In non-viscous flows, tangential velocity gradient at wall boundaries is set to zero. Atmospheric pressure is assumed at free surface elevation. Measured

DOI: 10.1002/fld

laboratory or theoretical velocity distributions in the vertical direction are adopted as inflow boundary conditions. Sommerfield radiation boundary condition together with sponge layer technique is implemented at outflow boundaries to eliminate wave reflection. As suggested by Yuan and Wu [13], a modified version of artificial damping term representing the sponge layer is used at the right hand side of Equation (5)

$$\left[\alpha\left(\frac{x-x_0}{l}\right)^2\left(\frac{z_b-z}{z_b-z_f}\right)\right]u, \quad x \geqslant x_0 \tag{10}$$

where x_0 is the beginning point of the sponge layer; l is the length of the sponge layer; z_f and z_b stand for the free surface and the bottom, respectively; and α is the damping strength coefficient. If $x < x_0$ the artificial damping term is set to zero.

At the end of the sponge layer, the following radiation boundary condition is applied where ϕ is any flow parameter which can be ξ, u, or w and c is the wave celerity.

$$\frac{\partial\phi}{\partial t} + c\frac{\partial\phi}{\partial x} = 0 \tag{11}$$

3. NUMERICAL METHOD

In this study, a finite volume approximation is used to discretize the governing equations and boundary conditions. A staggered grid mesh in sigma coordinate system with a set of $M \times N$ cells, respectively, in longitudinal and vertical direction is employed. The sigma coordinate system is a special non-orthogonal curvilinear system, which fits the surface and bottom boundaries of the domain. The major assumptions for this system are the constant number of vertical grids along the whole domain and the curvature applying only in the longitudinal direction. It should be stressed that in the present finite volume model the term 'sigma coordinate' refers to the special grid layout applied to the computational domain and no transformation of equations have been applied as required by finite difference approach. After each time step, the grid layout is modified to fit the new surface elevation boundary.

The velocity components are defined at the sides of each cell, the pressure defined at the cell centre, and surface and bottom elevations are defined at the centre of the upper and lower side of the corresponding cells of the water columns, respectively. Figure 2 illustrates the location of the main variables.

3.1. Derivative approximations

A common approach in the application of sigma coordinates is to transform the governing equations from Cartesian into the sigma coordinate system [7, 12] and then discretize the resulting equations. In this study 'finite volume' method has been deployed whereby mass and momentum are fully conserved.

The x derivatives of an arbitrary quantity φ and a control volume having nj edges, being expressed as

$$\frac{\partial\varphi}{\partial x} \approx \sum_{j=1}^{nj}\frac{\varphi_j \Delta z_j}{\mathrm{Ar}} \tag{12}$$

DOI: 10.1002/fld

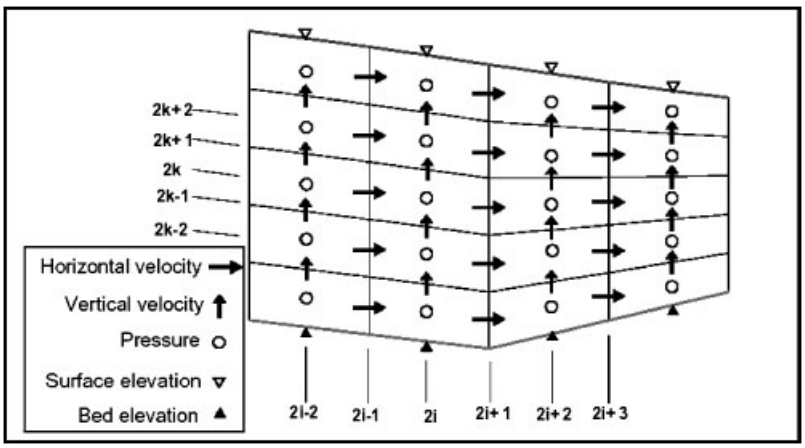

Figure 2. Presentation of staggered grids and the positions of the variables.

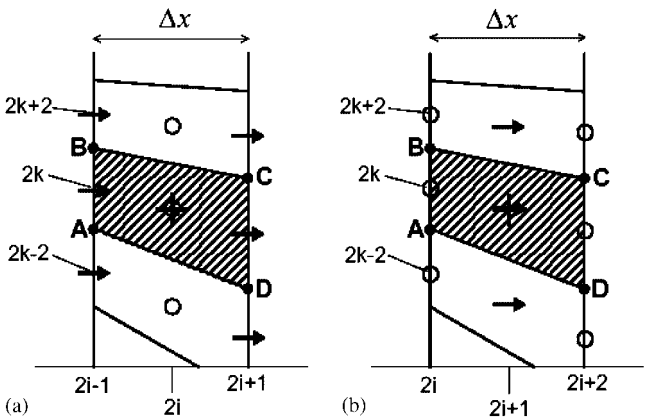

Figure 3. Presentation of the surrounding grids of: (a) even grids; and (b) odd grids, involved in x derivative calculation.

where φ_j and Δz_j refer to the average values of φ on the jth edge and the projected length of the jth edge in the z direction, respectively, and Ar is the area of the control volume. Applying the above relationship to the control volume presented in Figure 3(a), and calculating the values of $u_{2i,2k+1}$ and $u_{2i,2k-1}$ from the average value of the four surrounding velocities, then x derivative of the horizontal velocity around the point $(2i, 2k)$ may be written as

$$\left(\frac{\partial u}{\partial x}\right)_{2i.2k} \approx \sum_{j1=1}^{2} \sum_{j2=1}^{3} r_{j1,j2}^{2i,2k}\, u_{m_{2i}(j1),n_{2k}(j2)} \tag{13}$$

where

$$m_{2i}(1) = 2i - 1, \quad m_{2i}(2) = 2i + 1$$

DOI: 10.1002/fld

$$n_{2k}(1) = 2k-2, \quad n_{2k}(2) = 2k, \quad n_{2k}(3) = 2k+2$$

$$r^{2i,2k} = \begin{bmatrix} \dfrac{s_{2i,2k-1}}{4\Delta z_{2i}} & -\dfrac{\Delta z_{2i-1}}{\mathrm{Ar}} + \dfrac{s_{2i,2k-1}}{4\Delta z_{2i}} - \dfrac{s_{2i,2k+1}}{4\Delta z_{2i}} & -\dfrac{s_{2i,2k+1}}{4\Delta z_{2i}} \\ \dfrac{s_{2i,2k-1}}{4\Delta z_{2i}} & +\dfrac{\Delta z_{2i+1}}{\mathrm{Ar}} + \dfrac{s_{2i,2k-1}}{4\Delta z_{2i}} - \dfrac{s_{2i,2k+1}}{4\Delta z_{2i}} & -\dfrac{s_{2i,2k+1}}{4\Delta z_{2i}} \end{bmatrix}$$

$\mathrm{Ar} = \Delta x \Delta z_j$ is the area of the control volume, Δz_j is the space interval in the vertical direction of column $2i$, which for an equidistant sigma coordinate case, does not vary with k, $s_{2i,2k-1}$ and $s_{2i,2k+1}$ are the slopes of the longitudinal edges of the control volume, located at the location of $2i, 2k-1$ and $2i, 2k+1$ (i.e. lines BC and AD in Figure 3(a)), respectively. The derivatives of the pressure and other quantities located on the even column and even row numbers, as illustrated in Figure 3(b) can be derived from the above procedure by shifting the formulation from $2i$ to $2i+1$.

3.2. Numerical techniques

A finite volume method using a fractional step algorithm is deployed, which solves the governing equations in two major steps. In the first step, the momentum equations excluding the pressure gradient term are solved. This step is subdivided into two stages, namely 'advection' and 'diffusion' stages. In the second step, the continuity equation, together with the momentum equations without advection and diffusion terms are solved. In this step first, the vertical and horizontal velocity are expressed as functions of pressure. Second, substituting these relationships into the continuity equation yields a block tri-diagonal matrix system with the pressure as the unknown, which can be solved by a direct matrix solver without iteration using double sweep algorithm [10–13].

3.2.1. Step I. In the first step the momentum equations (5) and (6), are solved without the pressure gradient term. In stage one velocities are advected using the known velocity field at the previous time step n, to obtain the new intermediate velocity field $u^*$and w^* where

$$\frac{u^* - u^n}{\Delta t} = -\left[\frac{\partial(u^2)}{\partial x} + \frac{\partial(uw)}{\partial z}\right]^n \tag{14}$$

$$\frac{w^* - w^n}{\Delta t} = -\left[\frac{\partial(wu)}{\partial x} + \frac{\partial(w^2)}{\partial z}\right]^n \tag{15}$$

A Fromm [11, 17] upwind explicit numerical scheme is used to solve advection stage. In the next stage the diffusion terms are solved to find second intermediate velocities u^{**} and w^{**} wherein

$$\frac{u^{**} - u^*}{\Delta t} = \frac{\partial}{\partial x}\left(\nu_t \frac{\partial u^{**}}{\partial x}\right) + \frac{\partial}{\partial z}\left(\nu_t \frac{\partial u^{**}}{\partial z}\right) \tag{16}$$

$$\frac{w^{**} - w^*}{\Delta t} = \frac{\partial}{\partial x}\left(\nu_t \frac{\partial w^{**}}{\partial x}\right) + \frac{\partial}{\partial z}\left(\nu_t \frac{\partial w^{**}}{\partial z}\right) \tag{17}$$

Crank Nicholson scheme (CNS) is deployed to solve Equations (16) and (17). It has to be mentioned that none of the above-mentioned intermediate velocities necessarily satisfy the continuity equation.

DOI: 10.1002/fld

3.2.2. Step II. In the second step the continuity equation (1), together with the momentum equations without advection and diffusion terms are solved simultaneously giving

$$\left(\frac{\partial u}{\partial x}\right)^{n+1} + \left(\frac{\partial w}{\partial z}\right)^{n+1} = 0 \tag{18}$$

$$\frac{u^{n+1} - u^{**}}{\Delta t} + \left(\psi\left(\frac{\partial P^*}{\partial x}\right)^{n+1} + (1-\psi)\left(\frac{\partial P^*}{\partial x}\right)^{n}\right) = 0 \tag{19}$$

$$\frac{w^{n+1} - w^{**}}{\Delta t} + \left(\psi\left(\frac{\partial P^*}{\partial z}\right)^{n+1} + (1-\psi)\left(\frac{\partial P^*}{\partial z}\right)^{n}\right) = 0 \tag{20}$$

Using Equations (19) and (20) and applying the derivative definitions, the horizontal and vertical velocities can be written in the following form:

$$u^{n+1}_{2i-1.2k} = d_{2i-1.2k} - \psi\Delta t \sum_{j1=1}^{2}\sum_{j2=1}^{3} r^{2i-1,2k}_{j1,j2} P^{*n+1}_{m_{2i-1}(j1),n_{2k}(j2)} \tag{21}$$

$$w^{n+1}_{2i.2k-1} = d_{2i.2k-1} - \psi\Delta t\left(\frac{P^{*n+1}_{2i.2k} - P^{*n+1}_{2i.2k-2}}{\Delta z_{2i}}\right) \tag{22}$$

where

$$d_{2i-1,2k} = u^{**}_{2i-1,2k} - (1-\psi)\Delta t \sum_{j1=1}^{2}\sum_{j2=1}^{3} r^{2i-1,2k}_{j1,j2} P^{*n}_{m_{2i-1}(j1),n_{2k}(j2)} \tag{23}$$

$$d_{2i,2k-1} = w^{**}_{2i,2k-1} - (1-\psi)\Delta t\left(\frac{P^{*n}_{2i,2k} - P^{*n}_{2i,2k-2}}{\Delta z_{2i}}\right) \tag{24}$$

The weighting factor ψ, is taken as 0.5. Equations (21) and (22) define each velocity component in terms of the pressure located upstream and downstream of these velocity components, respectively. By substituting these values into the continuity equation (18), the velocities can be eliminated. To do so, first the derivatives of the velocities at the new time level $n+1$ can be expressed for the new velocities as defined by Equations (21) and (22), respectively, as

$$\begin{aligned}\left(\frac{\partial u}{\partial x}\right)^{n+1}_{2i.2k} &\approx \sum_{j1=1}^{2}\sum_{j2=1}^{3} r^{2i,2k}_{j1,j2} u^{n+1}_{m_{2i}(j1),n_{2k}(j2)} \\ &= \sum_{j1=1}^{2}\sum_{j2=1}^{3} r^{2i,2k}_{j1,j2} d_{m_{2i}(j1),n_{2k}(j2)} \\ &\quad - \psi\Delta t \sum_{j1=1}^{2}\sum_{j2=1}^{3} r^{2i,2k}_{j1,j2}\left(\sum_{j3=1}^{2}\sum_{j4=1}^{3} r^{m_{2i}(j1),n_{2k}(j2)}_{j3,j4} P^{*n+1}_{m_{m_{2i}(j1)}(j3),n_{n_{2k}(j2)}(j4)}\right)\end{aligned} \tag{25}$$

$$\left(\frac{\partial w}{\partial z}\right)^{n+1}_{2i.2k} \approx \frac{d_{2i,2k+1} - d_{2i,2k-1}}{\Delta z_{2i}} - \frac{\psi\Delta t}{(\Delta z_{2i})^2}(P^{*n+1}_{2i.2k+2} - 2P^{*n+1}_{2i.2k} + P^{*n+1}_{2i.2k-2}) \tag{26}$$

DOI: 10.1002/fld

Substituting Equations (25) and (26) into the continuity equation (18), the velocities are eliminated giving an equation in terms of the pressures as

$$\psi\Delta t \sum_{j1=1}^{2}\sum_{j2=1}^{3} r_{j1,j2}^{2i,2k}\left(\sum_{j3=1}^{2}\sum_{j4=1}^{3} r_{j3,j4}^{m_{2i}(j1),n_{2k}(j2)} P^{*n+1}_{m_{m_{2i}(j1)}(j3),n_{n_{2k}(j2)}(j4)}\right)$$

$$+\frac{\psi\Delta t}{(\Delta z_{2i})^2}(P^{*n+1}_{2i.2k+2} - 2P^{*n+1}_{2i.2k} + P^{*n+1}_{2i.2k-2})$$

$$= \sum_{j1=1}^{2}\sum_{j2=1}^{3} r_{j1,j2}^{2i,2k} d_{m_{2i}(j1),n_{2k}(j2)} + \frac{d_{2i,2k+1} - d_{2i,2k-1}}{\Delta z_{2i}} \tag{27}$$

3.2.3. Water surface condition and the pressure equation of the upper layer. The following equation can be written for the mass continuity for the column $2i$:

$$\frac{\xi^{n+1}_{2i} - \xi^{n}_{2i}}{\Delta t} + \frac{1}{\Delta x}\sum_{k=1}^{nk}(\theta\Delta z_{2i+1}u^{n+1}_{2i+1,2k} - \theta\Delta z_{2i-1}u^{n+1}_{2i-1,2k} + (1-\theta)\Delta z_{2i+1}u^{n}_{2i+1,2k}$$

$$-(1-\theta)\Delta z_{2i-1}u^{n}_{2i-1,2k}) = 0 \tag{28}$$

where nk is the number of layers. The implicit weighting factor θ, is taken as 0.5. If hydrostatic pressure assumption is accepted for the top layer

$$\xi^{n+1}_{2i} = \frac{P^{*n+1}_{2i.2nk}}{g}$$

The idea of applying hydrostatic assumption at the top layer under a staggered grid mesh has been addressed [6, 8, 10, 11]. Apparent phase error is observed as a result of adopting this assumption. In contrast, by applying fully non-hydrostatic pressure at the top layer, the calculated wave amplitude and phase are significantly improved and are well compared with the analytical solutions [12, 13]. The method applied by Yuan and Wu [12, 13], explicitly expresses the top-layer pressure in terms of hydrostatic pressure and vertical acceleration components. In the present study the top layer pressure gradient and vertical accelerations are treated implicitly, similar to the solution of lower layers, by implementing free surface dynamic and kinematic boundary conditions. Following the CNS, vertical momentum equation (20) in column $2i$ from the centre of top layer, to the free surface is approximated by

$$\frac{w^{n+1}_{2i.T} - w^{**}_{2i.T}}{\Delta t} + \psi\left(\frac{P^{*n+1}_{2i.S} - P^{*n+1}_{2i.2nk}}{\Delta z_{2i}/2}\right) + (1-\psi)\left(\frac{P^{*n}_{2i.S} - P^{*n}_{2i.2nk}}{\Delta z_{2i}/2}\right) = 0 \tag{29}$$

where $w^{n+1}_{2i.T} = (w^{n+1}_{2i.2nk-1} + w^{n+1}_{2i.2nk+1})/2$ is vertical velocity at top-layer; $w^{**}_{2i.T} = (w^{**}_{2i.2nk-1} + w^{**}_{2i.2nk+1})/2$ is intermediate vertical velocity at top-layer, obtained after step I; $P^{*n+1}_{2i.S} = g\xi^{n+1}_{2i}$

DOI: 10.1002/fld

and $P^{*n}_{2i.S} = g\xi^n_{2i}$ are pressure at surface water level. By substituting them into Equation (29)

$$\frac{w^{n+1}_{2i.2nk-1} + w^{n+1}_{2i.2nk+1} - w^{**}_{2i.2nk-1} - w^{**}_{2i.2nk+1}}{2\Delta t} + \psi\left(\frac{g\xi^{n+1}_{2i} - P^{*n+1}_{2i.2nk}}{\Delta z_{2i}/2}\right)$$

$$+ (1-\psi)\left(\frac{g\xi^{n}_{2i} - P^{*n}_{2i.2nk}}{\Delta z_{2i}/2}\right) = 0 \tag{30}$$

Substituting ξ^{n+1}_{2i} from Equation (28); $u^{n+1}_{2i-1.2k}$ from Equation (21); $w^{n+1}_{2i.2nk-1}$ from Equation (22); and $w^{n+1}_{2i.2nk+1}$ from continuity Equation (18), into Equation (30), the velocities are eliminated and the pressure equation of the upper layer is obtained as follows:

$$+\frac{\psi\Delta t.\Delta z_{2i}}{2\Delta t}\sum_{j1=1}^{2}\sum_{j2=1}^{3} r^{2i,2nk}_{j1,j2}\sum_{j3=1}^{2}\sum_{j4=1}^{3} r^{m_{2i}(j1),n_{2nk}(j2)}_{j3,j4} P^{*n+1}_{m_{m_{2i}(j1)}(j3),n_{n_{2nk}(j2)}(j4)} - \frac{3\psi}{\Delta z_{2i}} P^{*n+1}_{2i.2nk}$$

$$+\frac{\psi}{\Delta z_{2i}} P^{*n+1}_{2i.2nk-2} + \frac{2g\theta\Delta z_{2i+1}(\psi\Delta t)^2}{\Delta z_{2i}\Delta x}\sum_{k=1}^{nk}\sum_{j1=1}^{2}\sum_{j2=1}^{3} r^{2i+1,2k}_{j1,j2} P^{*n+1}_{m_{2i+1}(j1),n_{2k}(j2)}$$

$$-\frac{2g\theta\Delta z_{2i-1}(\psi\Delta t)^2}{\Delta z_{2i}\Delta x}\sum_{k=1}^{nk}\sum_{j1=1}^{2}\sum_{j2=1}^{3} r^{2i-1,2k}_{j1,j2} P^{*n+1}_{m_{2i-1}(j1),n_{2k}(j2)}$$

$$= +\frac{2\psi g\Delta t(1-\theta)}{\Delta z_{2i}\Delta x}\sum_{k=1}^{nk}(\Delta z_{2i+1}u^{n}_{2i+1,2k} - \Delta z_{2i-1}u^{n}_{2i-1,2k}) + \frac{w^{**}_{2i.2nk-1}}{2\Delta t} + \frac{w^{**}_{2i.2nk+1}}{2\Delta t}$$

$$+\frac{2(1-\psi)}{\Delta z_{2i}} P^{*n}_{2i.2nk} - \frac{2g}{\Delta z_{2i}}\xi^{n}_{2i} - \frac{d_{2i.2nk-1}}{\Delta t} + \frac{\Delta z_{2i}}{2\Delta t}\sum_{j1=1}^{2}\sum_{j2=1}^{3} r^{2i,2nk}_{j1,j2} d_{m_{2i}(j1),n_{2nk}(j2)}$$

$$+\frac{2\psi g\Delta t}{\Delta z_{2i}\Delta x}\left(\sum_{k=1}^{nk}\theta\Delta z_{2i+1}d_{2i+1.2k} - \sum_{k=1}^{nk}\theta\Delta z_{2i-1}d_{2i-1.2k}\right) \tag{31}$$

3.2.4. System of equations. By writing the equations of (27) for the pressure points of $2k$=2, 4, …, $2nk-2$ for each column, together with the pressure equation of the upper layer (31) for the last point (i.e. $2k = 2nk$), then the following system of equations can be obtained:

$$\overline{\overline{A}}^{1}_{i}\overline{P}^{*n+1}_{2i-2} + \overline{\overline{A}}^{2}_{i}\overline{P}^{*n+1}_{2i} + \overline{\overline{A}}^{3}_{i}\overline{P}^{*n+1}_{2i+2} = \overline{B_i} \tag{32}$$

where $\overline{P}^{*n+1}_{2i} = [P^{*n+1}_{2i,2}, P^{*n+1}_{2i,4}, \ldots, P^{*n+1}_{2i,2k}, \ldots, P^{*n+1}_{2i,2nk}]$ is the unknown pressure vector for column $2i$ and $\overline{\overline{A}}^{1}_{i}$, $\overline{\overline{A}}^{2}_{i}$ and $\overline{\overline{A}}^{3}_{i}$ are the 2D coefficient vectors for the pressures in columns $2i-2$, $2i$, and $2i+2$, respectively. For the upstream or downstream known pressure boundaries, only the diagonal members of the matrix $\overline{\overline{A}}^{2}_{bou}$ have to be set to one, with all other members of the coefficient vectors being set to zero. In this case, the vector on the right hand side of the equation

DOI: 10.1002/fld

has to contain the known boundary pressures. For the case of a known velocity then the main procedure can be followed, together with some minor modification given as: (a) setting $r_{j1,j2}^{Bou,2k}=0$ and (b) setting $d_{Bou,2k}=u_{Bou,2k}$ where the index *Bou*, being an odd integer, denotes the boundary column number and $u_{Bou,2k}$ is the known boundary velocity.

3.2.5. Solution algorithm. A tri-diagonal block matrix system can be formed by writing Equation (32) for all the even columns giving

$$\begin{bmatrix} \overline{\overline{A}}_1^2 & \overline{\overline{A}}_1^3 & & & & & \\ \overline{\overline{A}}_2^1 & \overline{\overline{A}}_2^2 & \overline{\overline{A}}_2^3 & & & & \\ & \overline{\overline{A}}_3^1 & \overline{\overline{A}}_3^2 & \overline{\overline{A}}_3^3 & & & \\ & & \vdots & \vdots & \vdots & & \\ & & & \overline{\overline{A}}_i^1 & \overline{\overline{A}}_i^2 & \overline{\overline{A}}_i^3 & \\ & & & & \vdots & \vdots & \end{bmatrix} \begin{bmatrix} \overline{X}_1 \\ \overline{X}_2 \\ \overline{X}_3 \\ \vdots \\ \overline{X}_i \\ \vdots \end{bmatrix} = \begin{bmatrix} \overline{B}_1 \\ \overline{B}_2 \\ \overline{B}_3 \\ \vdots \\ \overline{B}_i \\ \vdots \end{bmatrix} \tag{33}$$

Here the unknowns are $\overline{X_i}=\overline{P}_{2i}^{*n+1}$. To solve this system of equations a procedure similar to the double sweep algorithm [10–13] can be applied, in which the elements are vectors instead of scalars.

Having calculated the pressure values the velocities can be calculated using Equations (21) and (22) and then the new surface elevation can be obtained by applying Equation (28).

3.2.6. Radiation boundary condition. The radiation boundary condition (11), is discretized as

$$\frac{(\phi_{IB}^{n+1}+\phi_{IB-2}^{n+1})-(\phi_{IB}^{n}+\phi_{IB-2}^{n})}{2\Delta t}+0.5c\left(\frac{\partial\phi}{\partial x}\right)_{IB-1}^{n+1}+0.5c\left(\frac{\partial\phi}{\partial x}\right)_{IB-1}^{n}=0 \tag{34}$$

where $IB=2M+1$ for $\phi=u$ and $IB=2M$ for $\phi=w$ or P^*. $(\partial\phi/\partial x)$, can be obtained by applying Equation (12).

4. MODEL VALIDATIONS

4.1. Linear progressive short wave in deep water

A linear progressive short wave in deep water assuming an inviscid flow is a good example for representing the effects of hydrodynamic pressure distribution on model results. The wave propagates from left to right along a 700 m long, 10 m deep wave flume, with the initial water elevation being set zero. A sinusoidal velocity distribution, with wave amplitude being $A=0.1$ (i.e. 1% of the water depth), is imposed at the left boundary to simulate the action of the hinge-type wave maker. A combination of a sponge layer and a radiation boundary condition is applied at the outflow boundary. The wave period is $T=3.588$ s. The analytical solution for linear wavelength is $L=20$ m and wave celerity is $c=5.575$ m/s. The linear wave theory is valid in the case since the wave steepness, $2\pi A/2L=0.031$. Details of analytical solutions of the linear progressive wave can be

DOI: 10.1002/fld

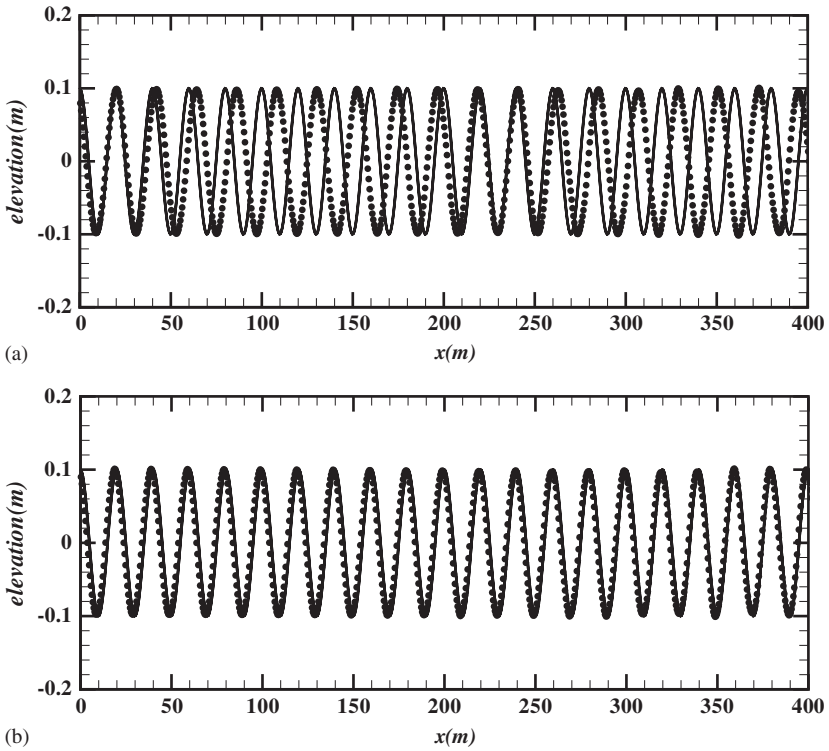

Figure 4. Comparisons of free-surface elevation for a linear progressive wave test ($t = 200$ s), between analytical solutions (solid lines) and numerical results (circles) from different models: (a) non-hydrostatic model with hydrostatic pressure assumption at the top layer; and (b) fully non-hydrostatic model.

found in [18]. The numerical parameters used in this test case are: $\Delta x = 1$ m, $\Delta z = 1$ m, $\Delta t = 0.1$ s. In Figure 4 different results obtained by applying a hydrostatic approximation at the top layer and the non-hydrostatic treatment of this layer are presented. Noticeable phase error is observed, when the hydrostatic approximation is applied at the top layer. On the contrary, non-hydrostatic pressure treatment at this layer yields a more accurate simulation of the wave amplitude and celerity. In Figure 5 comparison of dynamic pressure field and velocity are given. The velocities and dynamic pressure are also shown to be very close to the exact results.

4.2. Solitary wave propagation in a constant water depth

This test is performed to evaluate the capability of model in simulating non-linear terms i.e. advection, in NSE. According to the theory, a small amplitude solitary wave propagates in a constant water depth without changing its form, amplitude and velocities [19]. This is a basic test performed by many wave simulation models. Here we choose the same wave condition selected by Yuan and Wu [12]. In this test again an inviscid flow is considered. The amplitude of solitary wave, and the uniform water depth are taken as $A = 1.0$ m and $h = 10.0$ m, respectively. A uniform $M \times N = 1000 \times 10$ cells with the length of $L = 2000$ m is considered as computational domain and Δt is selected 0.1 s. $c = \sqrt{g(h + A)} = 10.388$ m/s is wave celerity based on theory, so the Courant

DOI: 10.1002/fld

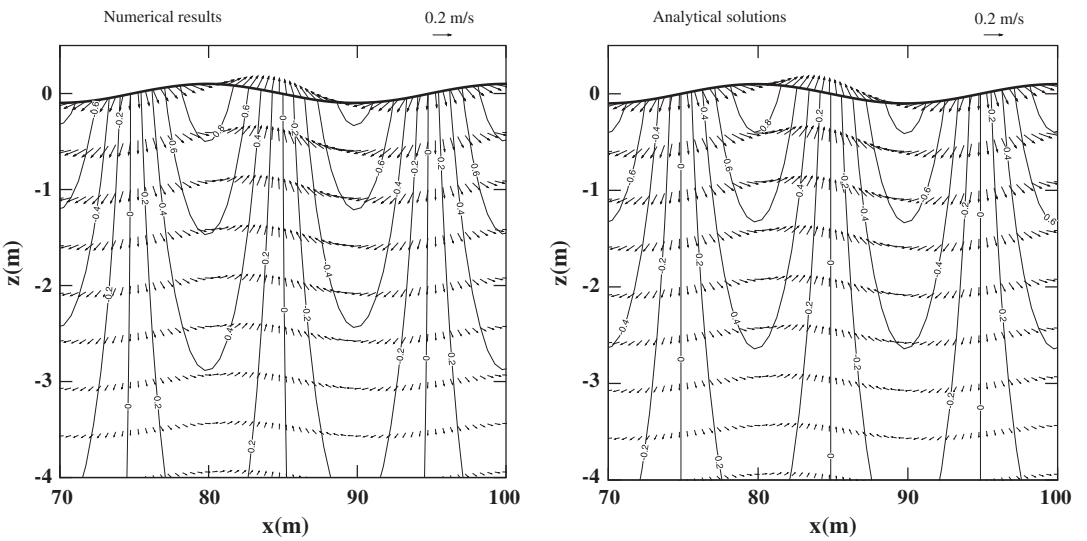

Figure 5. Comparison of dynamic pressure field and velocity for a linear progressive wave test between analytical solution and numerical results at $t = 200$ s. The unit of numbers on dynamic pressure contours is kPa.

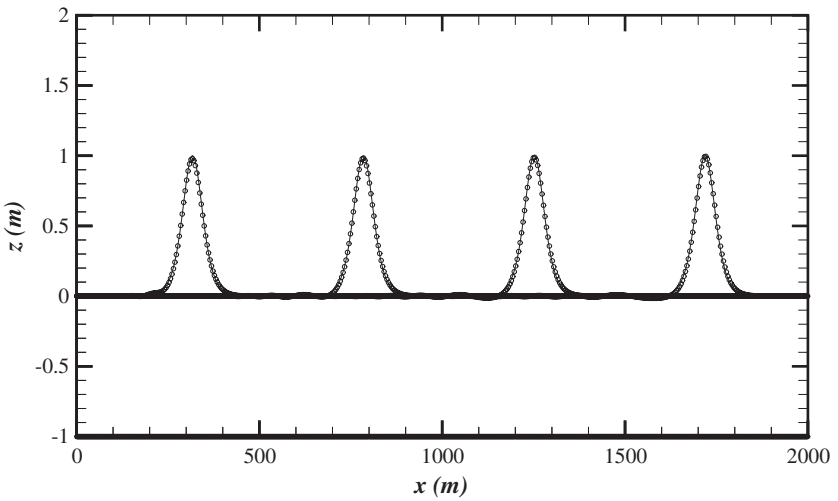

Figure 6. Comparisons of the free-surface elevation for solitary wave propagation in a constant water depth between numerical results (circles) and analytical solutions (solid line) at $t = 45$, 90, 135 and 180 s (wave propagation from left to right).

number is $Cr = c\Delta t/\Delta x = 0.519$. The velocity based on the analytical solution [20] is imposed as left boundary condition. At the right, the radiation boundary condition is applied. In order to start from a zero initial condition, the position of wave crest in $t = 0$ is selected at $x = -150$ m i.e. out of the computational domain. The comparison of the free-surface elevation between the numerical results and analytical solutions at $t = 45$, 90, 135 and 180 s, is demonstrated in Figure 6. The model

DOI: 10.1002/fld

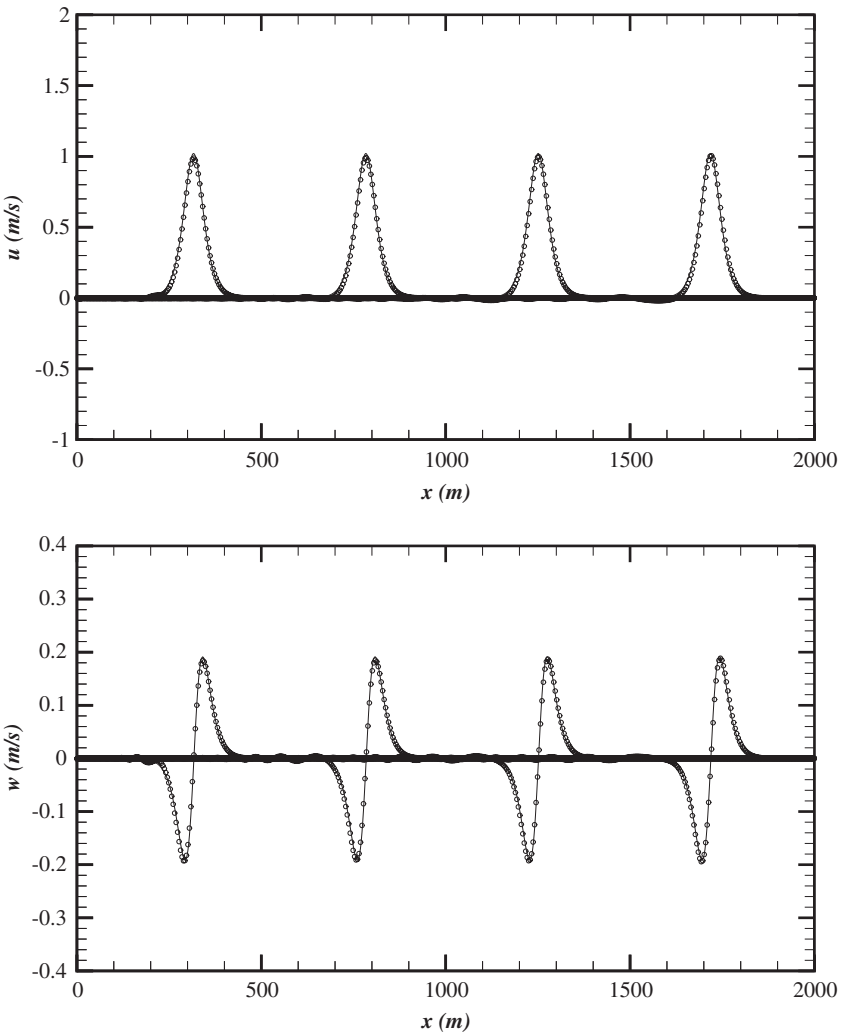

Figure 7. Comparison of u and w at the water surface for solitary wave propagation in a constant water depth between numerical results (circles) and analytical solutions (solid line) at $t = 45$, 90, 135 and 180 s (wave propagation from left to right).

gives good estimates of both the surface elevation and celerity. Figure 7 shows the comparisons of horizontal and vertical velocities at surface between the numerical results and analytical solutions. The numerical results are in very good agreement with analytical solutions, confirming the model predicts the hydrodynamic pressure and nonlinear terms very well. Figure 8 demonstrates some differences between analytical solution and the numerical results achieved by Yuan and Wu [12], especially in back side of the wave. In contrary the present numerical simulation clearly shows better agreement with analytical solution.

DOI: 10.1002/fld

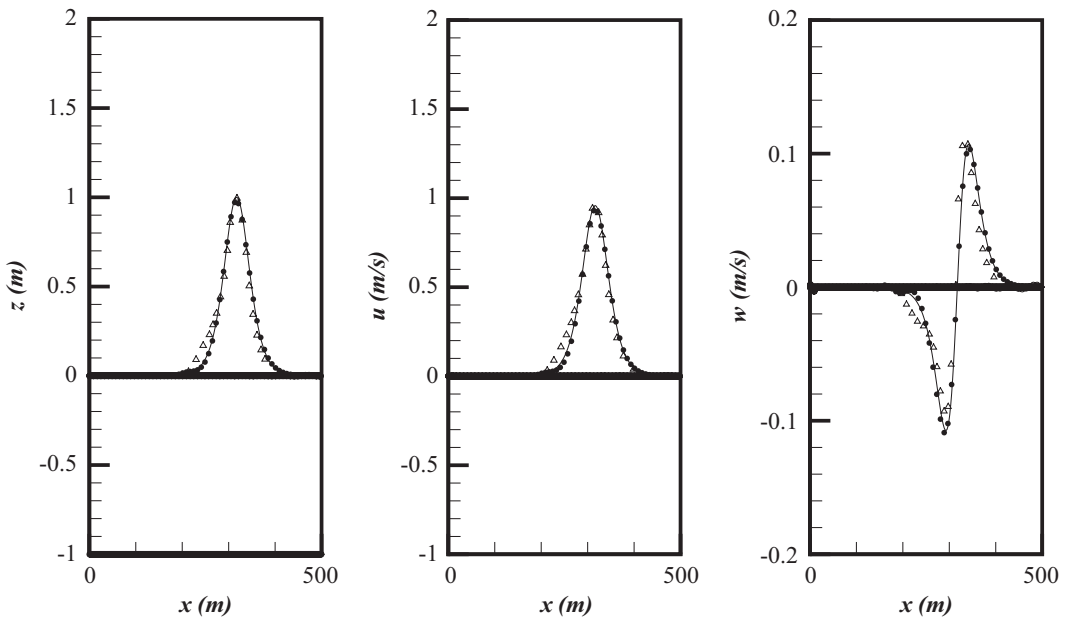

Figure 8. Comparison of the free-surface elevation, u and w at the middle elevation of the water depth for solitary wave propagation in a constant water depth between the numerical results of the present model (circles), analytical solutions (solid line) and numerical prediction of Yuan and Wu [12] (deltas) at $t = 45$.

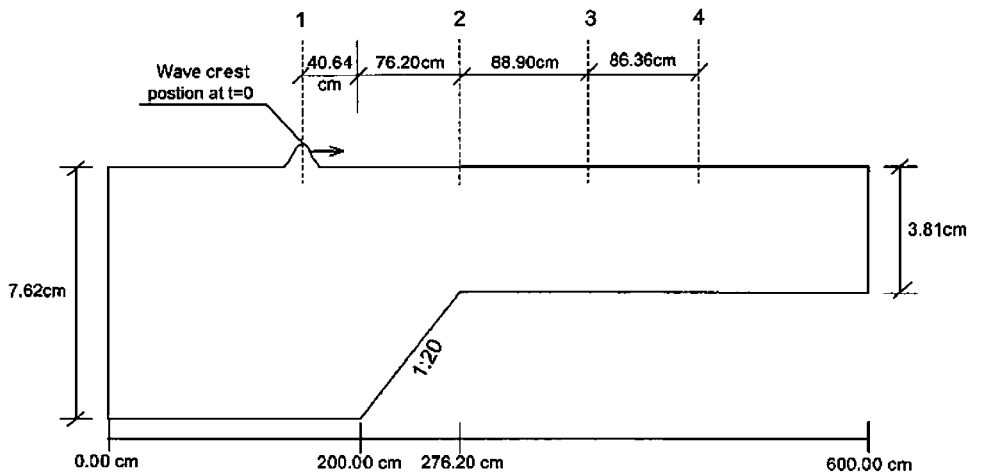

Figure 9. Flume geometry for solitary wave propagation over variable water depth.

4.3. Solitary wave propagation in a variable water depth

The ability of the model to simulate nonlinear wave propagation over uneven water depths is evaluated by comparing its results with a set of analytical/theoretical solution and experimental

DOI: 10.1002/fld

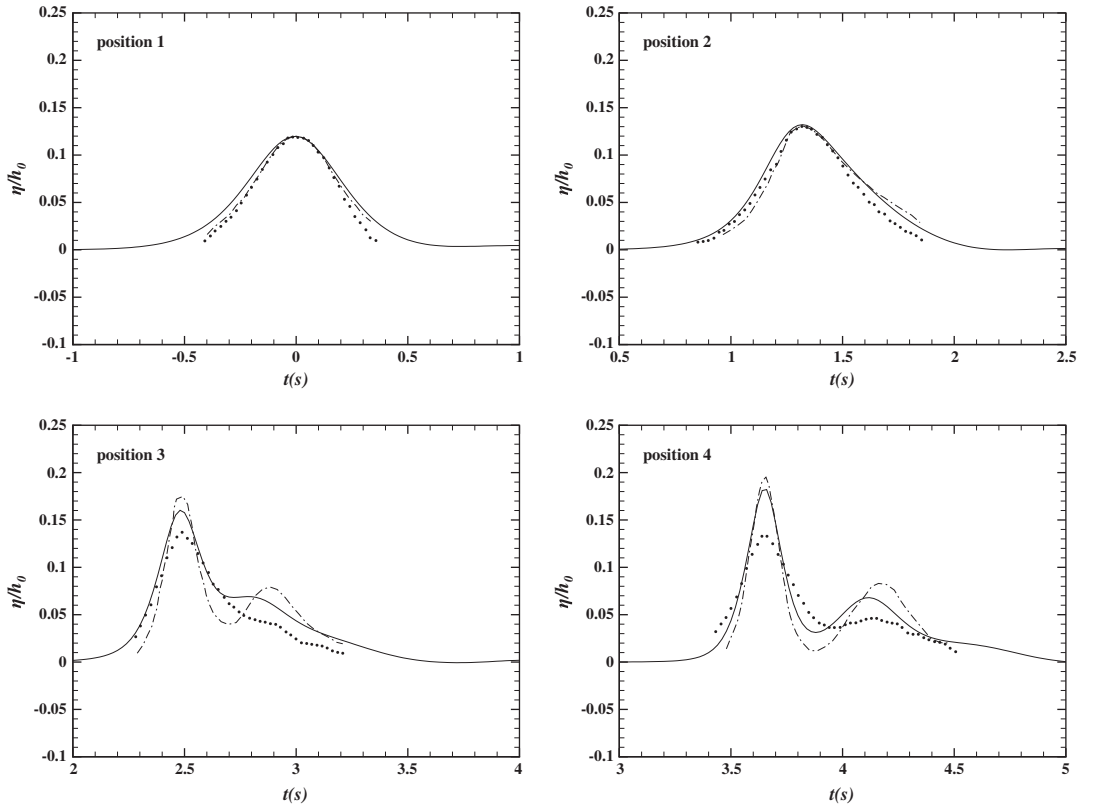

Figure 10. Comparison of the free-surface elevation for solitary wave propagation over variable water depth at locations 1, 2, 3 and 4 between numerical results (solid line), theoretical predictions (dashed line) and estimated experimental data for no viscous damping (circles).

data originally reported in Madsen and Mei [21] and referred by Yuan and Wu [12]. The so-called 'fission phenomenon' described in [19, 22] is the main feature that is investigated in this part of the study. The set-up of the experimental flume is shown in Figure 9. At the deep section of the flume, the wave height to water depth ratio is $A_0/h_0 = 0.12$, and the wave celerity is $c = \sqrt{g(h_0 + A_0)} = 0.915\,\mathrm{m/s}$. The viscosity is set to zero. The number of grid points in x and z directions ($M \times N$) are 600×10 and a time step of $\Delta t = 0.005\,\mathrm{s}$ is applied. The initial position of wave crest is located at $x = -0.8\,\mathrm{m}$. A known inflow is considered at the left and a radiation boundary is applied to the right.

The comparison of water surface profiles at four positions between numerical results, theoretical predictions and estimated experimental data for no viscous damping are presented in Figure 10. The numerical results exhibit the fission phenomenon quite good. Because of the difference in the predicted wave height by numerical and analytical calculations and that of experimental data, the wave celerity and the time that the wave crest reaches positions 3 and 4 are a little different in these three cases. Thus, in Figure 10, only the water surface profiles are compared. At position 4, the numerical results show a relative height of 151% for the larger wave and 55% for the smaller

DOI: 10.1002/fld

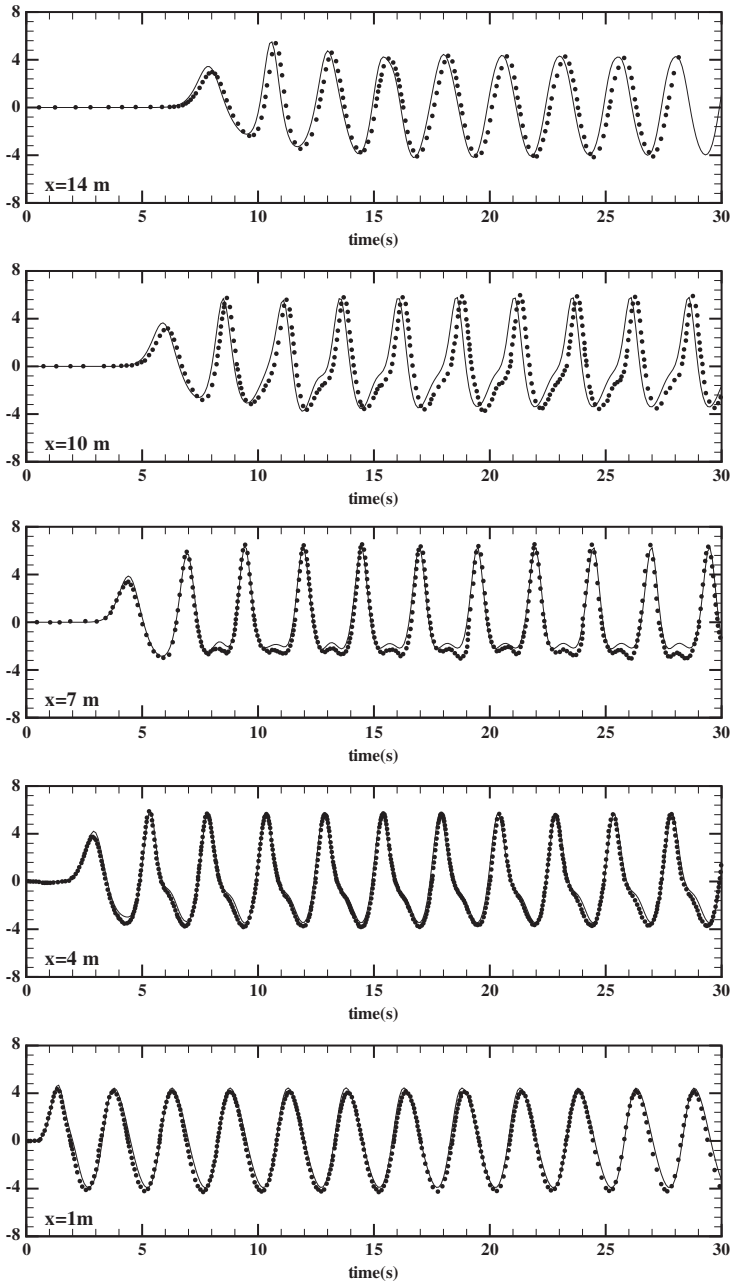

Figure 11. Comparisons of the free-surface elevation for nonlinear sinusoidal wave propagation along the wave channel between numerical results (solid line) and experimental data (circles). The amplitudes are expressed in cm.

DOI: 10.1002/fld

one, as compared to the initial wave height. This result matches other numerical and analytical predictions (e.g. 150 and 52% from Reference [22], 167 and 71% for a longer distance analytical approximation from Reference [21], 145 and 65% from Reference [12]).

4.4. Nonlinear short wave propagation in a constant water depth

A nonlinear progressive short wave in intermediate water depth assuming an inviscid flow is a test case used to validate the dynamic pressure and nonlinear behaviour predicted by the model against experimental data. The wave propagates from left to right along a 35.54 m long, 40 cm deep wave flume, with the initial water elevation being set to zero. A sinusoidal velocity distribution, with wave amplitude of $A = 4.2$ cm, is imposed at the left boundary to simulate the action of the hinge-type wave maker. A combination of a sponge layer and a radiation boundary condition is applied at the outflow boundary. The wave period is $T = 2.5$ s. The linear wave theory is invalid in this case. The numerical parameters used in this test case are: $\Delta x = 0.1$ m, $\Delta z = 0.05$ m, $\Delta t = 0.01$ s. Figure 11 shows comparisons of the predicted free-surface elevation along the flume with experimental data. The numerical results are in good agreement with experimental data reported by Chapalain *et al*. [23]. Close to the left boundary at $x = 0$ m, the wave profile is quasi-sinusoidal. At increasing distances an asymmetry develops that forms a small secondary crest in the trough of the primary wave at $x = 7.0$ m. The progression along the channel discloses a slow return to quasi-sinusoidal profile at $x = 14.0$ m. This structure of length equal to almost three times the wave length reappears beyond this point [23].

5. CONCLUSIONS

A fully dynamic numerical model is developed to simulate free surface flow in a two-dimensional vertical plane. Finite volume method with an implicit scheme on a sigma coordinate grid layout is applied which assures local and global mass conservation. The sigma coordinate grid layout is chosen as the computational mesh, which enables the model to simulate free-surface flows over irregular geometries. The proposed implicit treatment of non-hydrostatic pressure at the top layer, similar to the lower layers, makes the model free of any hydrostatic pressure assumption. It was found that this treatment enables the simulation of free surface elevation and wave celerity more accurately.

The numerical solution consists of a 'projection method' which solves the momentum equation without the pressure term in the first step. This step is called the 'advection–diffusion' step. In the second step the continuity and the momentum equations with only the pressure term are solved. A block tri-diagonal system of equations in terms of the pressure as the unknown is the result of this step which can be solved directly with no iteration required. The main bulk of the CPU time is spent for second step. Deploying time splitting method and excluding nonlinear terms in this step reduces the size of matrix system noticeably and decreases the execution time. Furthermore, one is free to use different numerical schemes for each step e.g. explicit upwind scheme for advection, implicit central method for diffusion. Because of the fast double sweep algorithm used in solving the tri-diagonal system of equations, it can be presumed that this model performs faster as compared to the models using iterative techniques.

The model is validated by several free surface tests with noticeable vertical accelerations. In modelling progressive linear short wave the results for free-surface elevation, wave celerity, velocities and dynamic pressure are in close agreement with analytical. In the case of solitary

DOI: 10.1002/fld

wave propagation in a constant water depth, the model accurately predicts free-surface elevation and velocities. Satisfactory predictions for solitary wave propagation over variable water depth are obtained which shows the ability of the model for simulating non-linear wave propagation in shoaling region. At last in the test of nonlinear progressive short wave, close agreement between numerical results and experimental data is observed which assures the capability of model for simulating non-linear short wave with significant vertical acceleration.

The extension of the present 2DV to a fully 3D model is in progress by the authors.

ACKNOWLEDGEMENTS

The work reported herein was supported by a grant from the Water Resources Management Co. under the Project Number RIV1-83084 and the Faculty of Civil Engineering, School of Engineering, University of Tehran. Their support is gratefully acknowledged.

REFERENCES

1. Chorin AJ. Numerical solution of the Navier–Stokes equations. *Mathematics of Computation* 1968; **22**:745–762.
2. Guermond JL, Quartapelle L. On stability and convergence of projection methods based on pressure Poisson equation. *International Journal for Numerical Methods in Fluids* 1998; **26**:1039–1053.
3. Mahadevan A, Oliger J, Street R. A non-hydrostatic mesoscale ocean model. Part 1: Well posedness and scaling. *Journal of Physical Oceanography* 1996; **26**(9):1868–1880.
4. Stansby PK, Zhou JG. Shallow-water flow solver with non-hydrostatic pressure: 2D vertical plane problems. *International Journal for Numerical Methods in Fluids* 1998; **28**:541–563.
5. Casulli V. A semi-implicit finite difference method for non-hydrostatic, free-surface flows. *International Journal for Numerical Methods in Fluids* 1999; **30**:425–440.
6. Li B, Fleming C. Three-dimensional model of Navier–Stokes equations for water waves. *Journal of Waterway, Port, Coastal, and Ocean Engineering* (ASCE) 2001; 16–25.
7. Lin P, Li C. A σ-coordinate three-dimensional numerical model for surface wave propagation. *International Journal for Numerical Methods in Fluids* 2002; **38**:1045–1068.
8. Kocyigit MB, Falconer RA, Lin B. Three-dimensional numerical modeling of free surface flows with nonhydrostatic pressure. *International Journal for Numerical Methods in Fluids* 2002; **40**:1145–1162.
9. Chen X. A fully hydrodynamic model for three-dimensional, free-surface flows. *International Journal for Numerical Methods in Fluids* 2003; **42**(9):929–952.
10. Namin M, Lin B, Falconer R. An implicit numerical algorithm for solving non-hydrostatic free-surface flow problems. *International Journal for Numerical Methods in Fluids* 2001; **35**:341–356.
11. Namin M. A fully three-dimensional non-hydrostatic free surface flow model for hydro-environmental prediction. *Ph.D. Thesis*, Cardiff School of Engineering, Cardiff University, 2003.
12. Yuan HL, Wu CH. A two-dimensional vertical non-hydrostatic σ model with an implicit method for free-surface flows. *International Journal for Numerical Methods in Fluids* 2004; **44**:811–835.
13. Yuan HL, Wu CH. An implicit three-dimensional fully non-hydrostatic model for free-surface flows. *International Journal for Numerical Methods in Fluids* 2004; **46**:709–733.
14. Casulli V, Stelling GS. Numerical simulation of 3D quasi-hydrostatic free-surface flows. *Journal of Hydraulic Engineering* (ASCE) 1998; **124**(7):678–686.
15. Stelling G, Zijlema M. An accurate and efficient finite-difference algorithm for non-hydrostatic free-surface flow with application to wave propagation. *International Journal for Numerical Methods in Fluids* 2003; **43**:1–23.
16. Casulli V, Zanolli P. Semi-implicit numerical modeling of nonhydrostatic free-surface flows for environmental problems. *Mathematical and Computer Modeling* 2002; **36**(9–10):1131–1149.
17. Fromm JE. A method of reducing dispersion in convective difference scheme. *Journal of Computational Physics* 1968; **3**:176–184.
18. Dean RG, Dalrymple RA. *Water Wave Mechanics for Engineers and Scientists*. World Scientific: Singapore, 2000.
19. Mei CC. *The Applied Dynamics of Ocean Surface Waves*. Wiley Inter-science: New York, 1983.

DOI: 10.1002/fld

20. Sorensen RM. *Basic Coastal Engineering*. Kluwer Academic Publishers: New York, 1997.
21. Madsen OS, Mei CC. The transformation of a solitary wave over an uneven bottom. *Journal of Fluid Mechanics* 1969; **39**(4):781–791.
22. Woo SB, Liu PLF. A Petrov–Galerkin finite element model for one-dimensional fully non-linear and weakly dispersive wave propagation. *International Journal for Numerical Methods in Fluids* 2001; **37**:541–575.
23. Chapalain G, Cointe R, Temperville A. Observed and modeled resonantly interacting progressive water-waves. *Coastal Engineering* 1992; **16**:267–300.

DOI: 10.1002/fld